NANO LETTERS

Letter

pubs.acs.org/NanoLett

Voltage-Induced Switching Dynamics of a Coupled Spin Pair in a Molecular Junction

T. Saygun, J. Bylin, H. Hammar, and J. Fransson*

Department of Physics and Astronomy, Uppsala University, Box 516, 75120 Uppsala, Sweden

Supporting Information

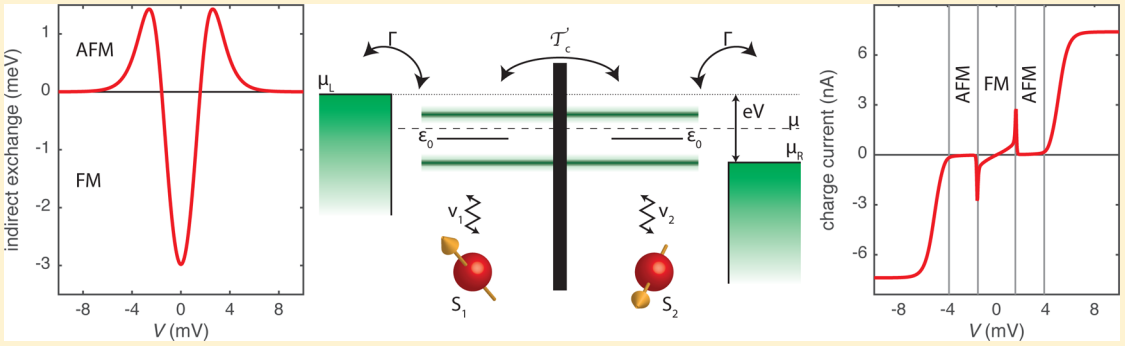

ABSTRACT: Molecular spintronics is made possible by the coupling between electronic configuration and magnetic polarization of the molecules. For control and application of the individual molecular states, it is necessary to both read and write their spin states. Conventionally, this is achieved by means of external magnetic fields or ferromagnetic contacts, which may change the intentional spin state and may present additional challenges when downsizing devices. Here, we predict that coupling magnetic molecules together opens up possibilities for all electrical control of both the molecular spin states as well as the current flow through the system. By tuning between the regimes of ferromagnetic and antiferromagnetic exchange interaction, the current can be at least an order of magnitude enhanced or reduced. The effect is susceptible to the tunnel coupling and molecular level alignment that can be used to achieve current rectification.

KEYWORDS: *Magnetic molecules, voltage-induced switching, magnetic exchange interaction, rectification*

Molecular spintronics is a field that aims to merge the flexibility of synthetic design of molecular compounds with novel functionalities offered by magnetic properties in conjunction with electronics circuits.[1] Magnetically active molecules have been used to demonstrate spin valve effect using external magnetic fields,[2] stochastic switching between high and low conductive states by transitions between spin singlet and triplet ground states,[3−6] controlled transport properties via paramagnetic atoms,[7] as well as their potential for quantum-based computation.[8−13] Arrays of magnetic molecules inserted between conducting leads, moreover, provide an important forum to investigate fundamental magnetic properties of finite one-dimensional Ising or Heisenberg chains[14−16] as well as potential for electrical and thermal control of the magnetic state. Certain classes of molecules, for example, metal-phthalocyanines (MPc) and metal-porhyrins (MP) present chemical stability with specific optical and electrical properties making them highly appreciated for technological applications including organic field effect transistors,[17,18] light-emitting devices[19,20] and photovoltaic cells,[21] and for fundamental studies.[7,22−27]

While incorporation of magnetic elements in molecular compounds can have a significant effect on the overall molecular transport properties,[7] the main established route to spintronics manipulations entails external magnetic fields[2] or ferromagnetic electrodes,[28,29] often exploiting spin transfer torques from spin-polarized scattering[30] or Coulomb interaction.[31] Here, we propose a different route to molecular spintronics based on voltage-induced control of magnetic interactions that allows for all electrical control of the transport properties. Deriving from local exchange interactions between the localized spin moments and the electrons in paramagnetic molecules, an indirect effective spin−spin interaction is generated between the molecular spin moments through the electron tunneling between the molecules.[32] In turn, the tunneling electrons are affected by the resulting spin state such that the system is driven into either a high or a low conductive regime, where the low conductive regime emerges from a novel form of spin singlet blockade phenomenon. Hence, we theoretically demonstrate that the voltage-controlled magnetic interactions can be used to tune between regimes of high and low conductance in paramagnetic molecular dimers, without using external magnetic fields or ferromagnetic leads. The effective spin−spin interaction is controlled by the energies of

Received: February 12, 2016
Revised: March 23, 2016
Published: March 24, 2016

DOI: 10.1021/acs.nanolett.6b00628
Nano Lett. 2016, 16, 2824−2829

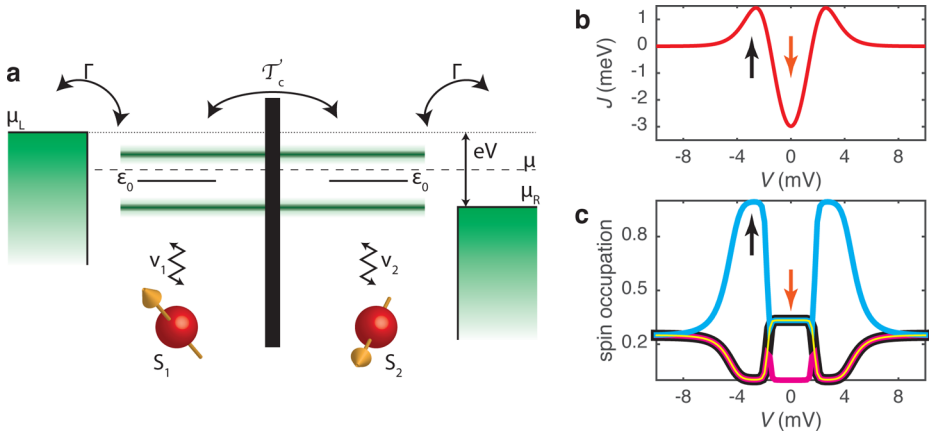

Figure 1. (a) Molecular dimer of paramagnetic molecules. An electron (at energy ε_0) in each molecule interacts with the localized spin moment ($\mathbf{S}_n$, n = 1,2) via exchange (v_n) with the electron in the adjacent molecule (tunneling rate $\mathcal{T}_c$) and with electrons in the left/right electrode (coupling Γ). The left/right nonmagnetic electrode is characterized by its electrochemical potential ($\mu_{L/R}$). Effective molecular orbitals ($\varepsilon_0 \pm \mathcal{T}_c$) emerge from intermolecular tunneling. (b) Effective exchange interaction between the localized spin moments as a function of the voltage bias V. (c) Occupation of the states of the spin dimer. The cyan curve represents the occupation of the lowest energy eigenstate of the spin dimer which changes character between spin singlet and spin triplet states as a function of the voltage bias. Other colors analogously represent the occupation of the consecutively higher energy eigenstates. Around equilibrium three states are degenerate and form the spin triplet. Calculations have been made at T = 4 K for ε_0 = 0, $\mathcal{T}_c$ = 1 meV, v_n = 5 meV, and Γ = 1 meV. In panels b and c, the ferromagnetic and antiferromagnetic regimes of the spin dimer are indicated with red and black arrows, respectively.

the highest occupied molecular orbitals (HOMO) and/or the lowest unoccupied molecular orbitals (LUMO) in the individual molecules and the intermolecular tunneling rate $\mathcal{T}_c$. It is therefore possible to switch between high and low conductive states of the coupled molecules through variation of the electrical environment of the molecular structure, for example, gating or voltage bias. Finally, we show that molecular level misalignment between the individual molecules leads to an asymmetry between the ferromagnetic and antiferromagnetic regimes with respect to the voltage bias that in turn gives rise to a suppression of the conductance in one direction of the current flow.

An important aspect of our work is the demonstration of nonequilibrium properties that cannot be predicted solely from an equilibrium consideration. While tuning between the ferromagnetic and antiferromagnetic regimes can be achieved using a gate voltage, this ability does not imply that the same property can be accomplished under nonequilibrium conditions. Thus, a generic conclusion of our results is that nonequilibrium aspects have to be considered to fully comprehend and control the physical properties.

Effective Magnetic Interactions. Effective interactions between magnetic moments in solid materials as well as in chemical compounds where dipolar interactions can be ignored derive from local exchange interactions between the magnetic moment ($\mathbf{S}_m$) and the nearby electronic spin structure ($\mathbf{s}(\mathbf{r})$) $\mathcal{H}_K = \sum_m \int v(\mathbf{r}, \mathbf{r}_m)\mathbf{s}(\mathbf{r})\cdot\mathbf{S}_m \, d\mathbf{r}$, where $v(\mathbf{r},\mathbf{r}_m)$ is the exchange integral between delocalized and localized spin $\mathbf{s}(\mathbf{r})$ and $\mathbf{S}_m$, respectively. From this basic concept it can be deduced that the effective spin−spin interaction can be mapped onto the spin interaction Hamiltonian[32,33]

$$\mathcal{H}_S = \sum_{mn} \left(J_{mn}\mathbf{S}_m\cdot\mathbf{S}_n + \mathbf{S}_m\cdot\mathbb{I}_{mn}\cdot\mathbf{S}_n + \mathbf{D}_{mn}\cdot[\mathbf{S}_m \times \mathbf{S}_n]\right) \quad (1)$$

where J_{mn}, $\mathbf{D}_{mn}$, and $\mathbb{I}_{mn}$ denote the Heisenberg, Dzyaloshinski-Moriya, and Ising interaction parameters, respectively. The interaction parameters depend on the properties of the electronic structure surrounding the localized spin moments. Considering the interaction between different spins, $m \neq n$, it can be shown that the Heisenberg interaction, which is of isotropic nature, essentially depends on the charge density available to mediate the coupling between the spins and is generally finite in metallic materials as well as in the types of molecular compounds considered in a spintronics context. In terms of eq 1, the spins tend to align ferromagnetically whenever $J_{mn} < 0$ while an antiferromagnetic alignment is favored for $J_{mn} > 0$. The Ising interaction is anisotropic, which is a property that stems from a spin-polarized electronic structure, without which it vanishes. Analogously to the Heisenberg interaction, negative (positive) Ising interaction leads to ferromagnetic (antiferromagnetic) spins along the spin quantization axis of the electronic structure. Finally, the Dzyaloshinski-Moriya interaction, which is a source for spin noncollinearity, is finite only whenever both time-reversal and inversion symmetries are broken. Materials with finite spin−orbit coupling fulfill this requirement; however, in molecular compounds these two symmetries can be broken by using ferromagnetic electrodes under nonequilibrium conditions.[32] Among the self-interactions, $m = n$, the Ising interaction provides an anisotropic dipolar[28] field to the local spins provided that the surrounding electronic structure is spin-polarized. The Heisenberg interaction adds a constant shift of the total energy, since $[\mathbf{S}_m, \mathcal{H}_S] = 0$, while the contribution from the Dzyaloshinski-Moriya interaction vanishes since $\mathbf{S}_m \times \mathbf{S}_m = 0$. Hence, both these two self-interactions are uninteresting for variations in the spin excitation spectrum.

Here, we consider a dimer of equivalent paramagnetic molecules inserted in the junction between metallic leads, see Figure 1a. We model this setup using the Hamiltonian $\mathcal{H} = \mathcal{H}_M + \mathcal{H}_{int} + \mathcal{H}_L + \mathcal{H}_R + \mathcal{H}_T$. Here, $\mathcal{H}_M = \sum_\sigma [\sum_{m=1,2} \varepsilon_m d^\dagger_{m\sigma} d_{m\sigma} + \mathcal{T}_c(d^\dagger_{1\sigma} d_{2\sigma} + H.c.)]$, where $d^\dagger_{m\sigma}$ ($d_{m\sigma}$) creates (annihilates) an electron in the mth molecule at the energy $\varepsilon_m = \varepsilon_0$ and spin $\sigma = \uparrow,\downarrow$, whereas $\mathcal{T}_c$ defines the tunneling rate between the molecules. Internally in molecule m,

DOI: 10.1021/acs.nanolett.6b00628
Nano Lett. 2016, 16, 2824−2829

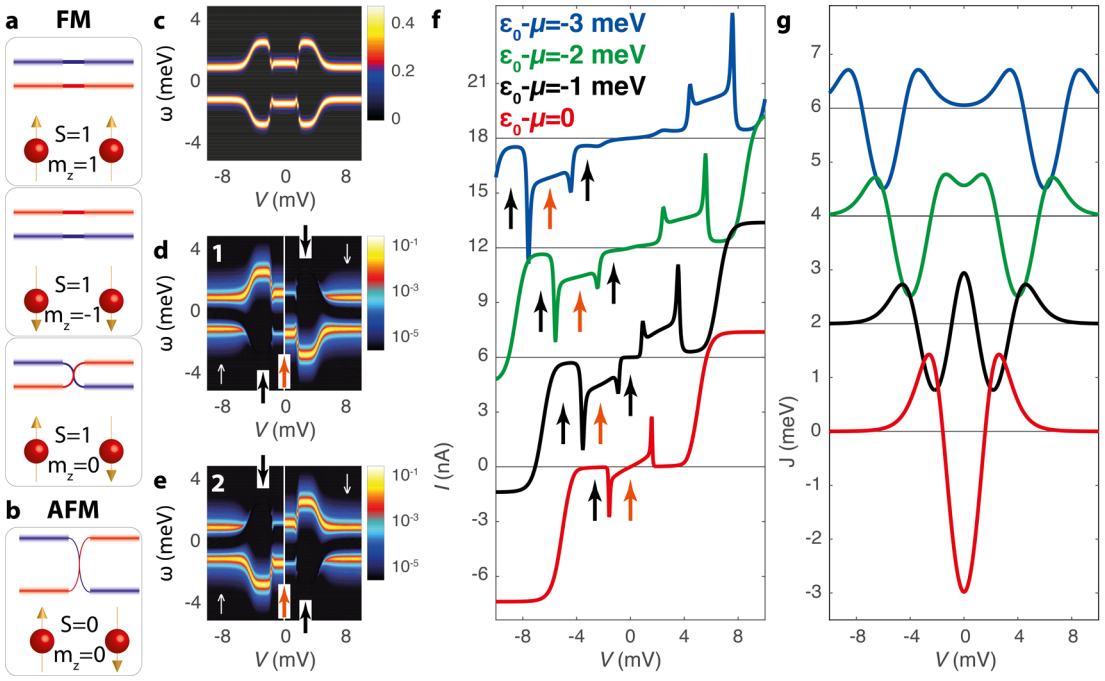

Figure 2. (a) The back-action of the spin triplet configurations on the molecular orbitals. The spin triplet configuration generates a delocalized DOS, resulting from the average of three degenerate spin configurations. (b) The back-action of the spin singlet configuration on the molecular orbitals causes a strongly localized spin-projected DOS. (c) Total density of electron states in the molecular dimer. (d,e) Molecule and spin-projected (indicated by white arrows) DOS of the left and right nongated ($\mu = 0$) molecules, respectively, as a function of the voltage bias V and energy ω. (f) Charge current through the molecular complex as a function of the voltage bias (V) for different gating conditions ($\varepsilon_0 - \mu = 0, -1, -2, -3$ meV). (g) Corresponding effective exchange interactions. The plots are offset for clarity (f,g). In panels d–f, the ferromagnetic and antiferromagnetic regimes of the spin dimer are indicated with red and black arrows, respectively. Parameters are as in Figure 1.

the localized spin moment $\mathbf{S}_m$ interacts with the electron spin $\mathbf{s}_m = \sum_{\sigma\sigma'} d^\dagger_{m\sigma}\boldsymbol{\sigma}_{\sigma\sigma'}d_{m\sigma'}/2$ via exchange $\mathcal{H}_{\text{int}} = \sum_m \nu_m \mathbf{s}_m\cdot\mathbf{S}_m$, where ν_m is the exchange integral, and we assume that $\nu_m = \nu$. We focus on the case with nonmagnetic leads, $\mathcal{H}_{\text{L/R}} = \sum_{\mathbf{k}\sigma\in\text{L/R}} \varepsilon_{\mathbf{k}} c^\dagger_{\mathbf{k}\sigma}c_{\mathbf{k}\sigma}$, where $c^\dagger_{\mathbf{k}\sigma}$ creates an electron in the left (L; $\mathbf{k} = \mathbf{p}$) or right (R; $\mathbf{k} = \mathbf{q}$) lead at the energy $\varepsilon_{\mathbf{k}}$ and spin σ. Tunneling between the leads and molecules is described by $\mathcal{H}_{\text{T}} = \sum_{\mathbf{p}\sigma} T_{\text{L}} c^\dagger_{\mathbf{p}\sigma}d_{1\sigma} + \sum_{\mathbf{q}\sigma} T_{\text{R}} c^\dagger_{\mathbf{q}\sigma}d_{2\sigma} + H.c.$ Hence, $\mathcal{H}_{\text{L}} + \mathcal{H}_{\text{R}} + \mathcal{H}_{\text{T}} + \mathcal{H}_{\text{M}}$ provides a spin-degenerate electronic structure that mediates the exchange interactions, which implies that both the Dzyaloshinski-Moriya and Ising interactions vanish ($\mathbf{D}_{mn} = 0$, $\mathbb{I}_{mn} = 0$) and we retain the isotropic Heisenberg interaction only. In this way, we treat the spin dimer as a closed system, that is, conserved number of particles for which the occupations of the states is given by the Gibbs distribution, which is influenced by the tunneling current that flows through the molecular complex. This setup pertains to, for example, MPc and MP where M denotes a magnetic transition metal atom, for example, Cr, Mn, Fe, Co, Ni, Cu, and can be realized in, for example, mechanically controlled break-junctions[7] and scanning tunneling microscope.[34,35] Having such systems in mind also justifies that we neglect spin–orbit coupling in the molecular orbitals, because such coupling essentially pertains to the d-electrons constituting the paramagnetic moment, and also that we consider the molecular levels in a single particle form, relevant for s- and p-electrons. In such setups, the effective magnetic interaction parameter J between the two spins can be calculated using the expression (see Supporting Information)

$$J = -\frac{\mathcal{T}_c^2}{8\pi}\nu^2\Gamma\int (f_{\text{L}}(\omega) + f_{\text{R}}(\omega))(\omega - \varepsilon_0)\frac{(\omega-\varepsilon_0)^2 - \mathcal{T}_c^2 - \left(\frac{\Gamma}{8}\right)^2}{\left|\left(\omega - \varepsilon_0 + \frac{i\Gamma}{8}\right)^2 - \mathcal{T}_c^2\right|^4}\,d\omega \quad (2)$$

where $\Gamma = \sum_{\chi=\text{L,R}}\Gamma^\chi$, with $\Gamma^\chi = 2\pi\sum_{\mathbf{k}\sigma\in\chi} T_\chi^2\delta(\omega-\varepsilon_{\mathbf{k}})$, is the coupling to the leads, and $f_{\text{L/R}}(\omega)$ is the Fermi function at the chemical potential $\mu_{\text{L/R}}$ of the left/right lead such that the voltage bias applied across the junction can be defined as $V = (\mu_{\text{L}} - \mu_{\text{R}})/e$. The voltage bias dependence of J is plotted in Figure 1b for the case with $\varepsilon_0 = 0$ (for other parameters, see the figure caption). Near equilibrium ($V \approx 0$), $\mu_{\text{R}} \approx \mu_{\text{L}} = \mu$, this integral gives a negative (ferromagnetic) value for J whenever μ lies between the upper and lower effective orbital energies $\varepsilon_0 \pm \mathcal{T}_c$ of the molecular dimer, indicated by the red arrow in Figure 1b. In this regime, the ground state of the spin dimer is a spin triplet, labeled by $|T;m = 0, \pm\rangle$ where T denotes the triplet and m is its projection. This is illustrated in Figure 1c, which shows the occupation number for the four possible states in the spin dimer corresponding to the evolution of J in panel b. The red arrow indicates that the three projections of the spin triplet are equally occupied (~1/3). With increasing voltage bias, μ_{L} and μ_{R} approach the orbital energies $\varepsilon_0 \pm \mathcal{T}_c$, which leads to a peaked positive (antiferromagnetic) J as $\mu_{\text{L/R}}$ sweeps through the orbital energies (indicated by the black arrow in Figure 1b). Hence, the spin dimer acquires a spin singlet ground state, $|S\rangle$, with nearly unit occupation as is indicated by the black arrow in Figure 1c. By further increasing the voltage bias, eventually both energies $\varepsilon_0 \pm \mathcal{T}_c$ lie between μ_{L} and μ_{R} and J remains

DOI: 10.1021/acs.nanolett.6b00628
Nano Lett. 2016, 16, 2824–2829

positive but approaching zero, which leads to that the ground state of the spin dimer becomes a superposition of the spin triplet and spin singlet states. In this regime, where $J \to 0$, the four states are equally occupied ($\sim$1/4) which can be seen in Figure 1c. It should be emphasized, however, that the total magnetic moment of the spin dimer vanishes for all voltages due to the absence of magnetic anisotropies.

An advantage with the present setup where we use nonspin-polarized leads compared to designs based on ferromagnetic leads is that the dipolar and quadrupolar fields considered in ref 28 here become vanishingly small. Therefore, the effective electron mediated spin−spin interactions dominates the properties and control of the molecular dimer.

Conductance States of Molecular Structure. By tuning between the regimes with ferromagnetic and antiferromagnetic J, the state of the spin dimer is dynamically switched between spin triplet and singlet configurations. Because of the local interaction between the spin moment and the electrons, this switching directly affects the conductance through the molecular dimer. In fact, the state of the spin dimer influences the conducting orbitals and splits the molecular energy levels $\varepsilon_0 \pm \mathcal{T}_c$ into $E_\pm = \varepsilon_0 \pm \tilde{T}_c/2$, where $\tilde{T}_c^2 = v^2\langle S_1^z - S_2^z\rangle^2 + 4\mathcal{T}_c^2$ is the mean field splitting induced by the local spin moments, and $\langle S_m^z\rangle$ is the molecule, or site, projected expectation value of the spin within the eigenbasis of the spin dimer. In the present case, these expectation values take the values $\langle S_1^z\rangle = -\langle S_2^z\rangle = S$ and $S/3$ in the antiferromagnetic and ferromagnetic regimes, respectively, where S denotes the spin moment. This antiparallel alignment of the spins agrees with the very definition of the spin singlet state, as well as for the paramagnetic configuration $|T,m = 0\rangle$ among the triplet states. The contributions to the expectation values from the ferromagnetic triplet states $|T,m = \pm 1\rangle$ cancel each other, however. Therefore, the ratio between the expectation values $|\langle S_1^z - S_2^z\rangle|$ for the ferromagnetic and antiferromagnetic regimes is 1/3, which corresponds to the different distributions of the occupation numbers among the triplet and singlet states within the respective regime. Hence, the splitting of the molecular energy levels in the ferromagnetic regime is smaller than in the antiferromagnetic regime. This is illustrated in Figure 2c, where we plot the total density of electron states (DOS) in the two molecules. In comparison, conventional spintronics crucially depend on magnetic fields. In order to obtain the splitting between the conducting states E_+ and E_-, which here is induced by $v|\langle S_1^z - S_2^z\rangle|$ with $v \sim 0.5$−20 meV,[36,37] one would have to apply a field strength of the order of $4|\langle S_1^z - S_2^z\rangle| - 170|\langle S_1^z - S_2^z\rangle|$T.

The main importance of the induced orbital splitting, however, is the distribution of the spectral weight of the molecular orbitals onto the individual molecules. This can be seen by analyzing the 2×2 matrix Green function (GF) for, for example, molecule 1, $\mathbf{G}^{(1)} = \{G^{(1)}_{\sigma\sigma'}\}_{\sigma\sigma'=\uparrow\downarrow}$, which can be written as

$$\mathbf{G}^{(1)}(\omega) = \frac{1}{2\tilde{T}_c}\sum_{s=\pm}\frac{\tilde{T}_c\sigma^0 - s2v\langle S_2^z\rangle\sigma^z}{\omega - E_s + \frac{i\Gamma}{8}} \tag{3}$$

where σ^z is a Pauli matrix whereas σ^0 is the identity. In the limit of small $\mathcal{T}_c$, the spectral weights of the component $G^{(1)}_{\uparrow\uparrow}$ around the energies E_+ and E_- are $v\langle S_1^z - 3S_2^z\rangle - 2\mathcal{T}_c^2/v\langle S_1^z - S_2^z\rangle$ and $v\langle S_1^z + S_2^z\rangle - 2\mathcal{T}_c^2/v\langle S_1^z - S_2^z\rangle$. Here, the former spectral weight is finite in both the antiferromagnetic and ferromagnetic regimes while the latter is finite only in the ferromagnetic regime and negligible in the antiferromagnetic. The distribution of the spectral weights for the component $G^{(1)}_{\downarrow\downarrow}$ is the opposite. Schematically, this is illustrated in Figure 2a,b, while in Figure 2d we plot the computed molecule and spin-projected DOS, $-\mathrm{Im}G^{(1)}_{\uparrow\uparrow(\downarrow\downarrow)}/\pi$ for positive (negative) voltage biases. Repeating the analysis for molecule 2, which GF is obtained from eq 3 by the replacements $\langle S_2^z\rangle \to \langle S_1^z\rangle$, $\sigma^z \to -\sigma^z$, and $\Gamma^L \to \Gamma^R$, shows that the distribution of the spectral weights is opposite to that of molecule 1, see Figure 2e, which shows the corresponding DOS for molecule 2. In particular, this means that $G^{(1)}_{\sigma\sigma}$ and $G^{(2)}_{\sigma\sigma}$ have a negligible (finite) overlap, or in other words the spin-projections of the electronic density are localized (delocalized) in the antiferromagnetic (ferromagnetic) regime, which has a large influence on the transport properties as we shall see next.

In the ferromagnetic regime, where the spin-projected DOS is delocalized in the molecular dimer, there are channels open for conduction which leads to a finite current flow. This is indicated by the red arrows in Figure 2f, where we plot the current I for different gating conditions ($\varepsilon_0 - \mu = 0, -1, -2, -3$ mV), see the Supporting Information for details concerning the current. The corresponding exchange interactions J are shown in Figure 2g. On the other hand, in the antiferromagnetic regime the spin-projected DOS is localized and because we assume spin conservative tunneling between the molecules this leads to that an electron with spin σ residing in molecule 1 has only a small probability to tunnel into molecule 2. Hence, the resulting current becomes severely suppressed, see Figure 2f (black arrows). The qualitative behavior of the current is the same in all four current traces, showing a high conductance in the ferromagnetic regime (red arrows) and a low conductance in the antiferromagnetic regime (black arrows) and we refer to the latter regime as a spin-singlet blockade. We stress the fact that because the dimer is constructed from paramagnetic molecules, this characteristic is independent of the spin quantization axis. The sharp current peaks separating the ferromagnetic and antiferromagnetic regimes result from a complete delocalization of the DOS when the exchange interaction parameter crosses between negative and positive values, which leads to a 4-fold degeneracy of the spin states.

With increasing voltage bias, the system evolves through regimes with different transport characteristics. First, in the nongated case ($\mu = 0$) for small voltage biases the high conductance ferromagnetic regime (Figure 2g) is subsequently followed by a low conductance state in the antiferromagnetic regime when increasing the voltage bias. As we saw above, the effective exchange interaction tends to become small by further increasing the voltage bias (Figure 2g) such that the spin dimer evolves into a new regime with 4-fold degenerate spin states. In this phase, the molecular orbitals are completely delocalized (Figure 2c,d), which permits an open flow of electrons through the molecular complex, yielding a significantly increased current, as can be seen in the current in the high bias regime (Figure 2f). Application of a gate voltage that shifts the energy levels with respect to μ leads to that the ferro- and antiferromagnetic regimes move to higher voltage biases (Figure 2f,g), because the molecular orbital energies may not lie on either side of μ in equilibrium but require a finite voltage bias to fulfill this condition. Therefore, for sufficiently large gating conditions, for example, $|\varepsilon_0 - \mu| \geq \mathcal{T}_c$, which is fulfilled for $\varepsilon_0 - \mu = -1$ meV, the system is antiferromagnetic in the low bias regime and only enter into the ferromagnetic regime for finite voltage biases (Figure 2f,g), which is followed by an

DOI: 10.1021/acs.nanolett.6b00628
Nano Lett. 2016, 16, 2824−2829

another antiferromagnetic regime for a further increase of the voltage bias. This illustrates a generic property of the system, namely, that the ferromagnetic regime is surrounded by antiferromagnetic regimes that allows for switching between high and low conductance properties by shifting to either smaller or larger voltage biases, a dual switching functionality. For even larger gating conditions, $\varepsilon_0 - \mu \gtrsim -2$ meV (Figure 2f,g), the system is initially in the highly conducting 4-fold degenerate regime at low voltage biases and only thereafter evolves through the antiferromagnetic, ferromagnetic, and antiferromagnetic regimes, respectively, with increasing voltage bias. This behavior illustrates the systematic shift of the ferromagnetic and antiferromagnetic regimes away from equilibrium to higher voltage biases with gating.

Nonequivalent Molecules and Rectification. In the antiferromagnetic regime, the spin-projected DOS are strongly localized to either molecule (Figure 3b, upper panel), as

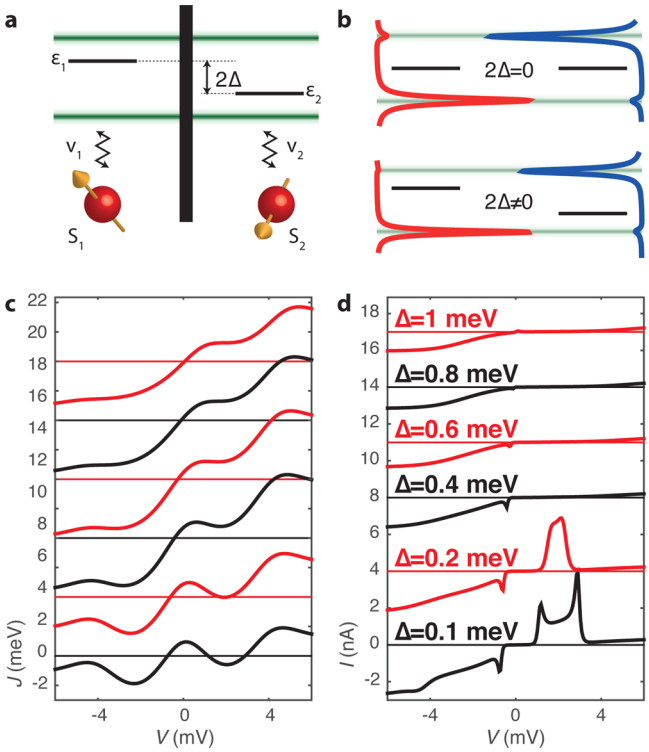

Figure 3. (a) Energy diagram of the nonequivalent molecules and the corresponding effective orbitals. The asymmetry is characterized by the level offset 2Δ. (b) Spatial distribution of the DOS for one spin-projection, illustrating the spatial asymmetry between the two molecules. (c) Effective exchange interaction as a function of the voltage bias for different asymmetric configurations of the molecular levels, $\varepsilon_n = \varepsilon_0 + (-1)^n\Delta$, n = 1,2, and $\Delta \in \{0.1, 0.2, 0.4, 0.6, 0.8, 1\}$ meV for $\varepsilon_0 - \mu = -1$ meV. (d) Corresponding charge currents. Plots c and d are offset for clarity. Parameters are as in Figure 2.

discussed above. The degree of localization can be further enhanced by replacing the molecular dimer with nonequivalent molecules in which the local electronic structure in each molecule is slightly different to one another (Figure 3a). The imposed asymmetry can be used to amplify the singlet blockade and in this way to achieve current rectification. By introducing a finite level offset between the orbital energies in the two molecules, the asymmetry of the spin-projected DOS can be fine-tuned into almost complete localization (Figure 3b, lower panel). The strongly asymmetric orbital configuration allows for fine-tuning the effective exchange such that it becomes ferromagnetic, for example, for negative voltage biases and antiferromagnetic for positive. This is illustrated in Figure 3c, which shows the effective exchange as a function of the voltage bias for increasing level offset Δ between the molecular orbital energies. By this separation of the ferromagnetic and antiferromagnetic regimes to negative and positive voltage biases, respectively, the system becomes an effective rectification device, which can be seen in the plots of the corresponding total currents I shown in Figure 3d, also see the Supporting Information. Here, for small level offsets $\Delta \leq 0.2$ meV, the spin dimer has ferromagnetic regimes on both sides of zero voltage bias (Figure 3c), such that the molecular system has a highly conducting range for negative and positive voltages. Moderately increasing the level offset, $\Delta \gtrsim 0.3$ meV completely removes the ferromagnetic regime for positive voltages that leads to an effective suppression of the current, hence, the system is strongly rectifying. We notice that rectification was recently robustly realized in molecular dimers,[38] however, arising from a completely different physical origin.

Conclusions. In conclusion, we predict that electrical control of the effective exchange interaction in molecular spin dimer complexes can be utilized to provide switching function of the system by tuning the system between ferromagnetic and antiferromagnetic regimes, a tuning that can be provided by the voltage bias and gate voltage. In effect, the triplet and singlet spin states in the molecular dimer leads to a either delocalized or localized spin-projected DOS such that the ferromagnetic regime becomes highly conducting whereas the conductance is suppressed in the antiferromagnetic. This property opens up possibilities for electrical switching between different states associated with dramatic changes in the differential conductance. For molecular complexes with individual gating or nonequivalent paramagnetic molecules, it is predicted that the properties can be fine-tuned for specific functional characteristics. Finite level offset between the molecular orbitals can, for instance, be used to create effective current rectification where the high and low conductance phases are controlled by spin triplet and spin singlet states of the molecular spin dimer.

■ ASSOCIATED CONTENT

Supporting Information

The Supporting Information is available free of charge on the ACS Publications website at DOI: 10.1021/acs.nanolett.6b00628.

Details of theoretical derivations and calculations. (PDF)

■ AUTHOR INFORMATION

Corresponding Author

*E-mail: Jonas.Fransson@physics.uu.se.

Notes

The authors declare no competing financial interest.

■ ACKNOWLEDGMENTS

We thank A. V. Balatsky, O. Eriksson, and A. Bergman for stimulating discussions and we acknowledge support from Vetenskapsrådet.

■ REFERENCES

(1) Bogani, L.; Wernsdorfer, W. *Nat. Mater.* **2008**, *7*, 179.

DOI: 10.1021/acs.nanolett.6b00628
Nano Lett. 2016, 16, 2824−2829

(2) Urdampilleta, M.; Klyatskaya, S.; Cleuziou, J.-P.; Ruben, M.; Wernsdorfer, W. *Nat. Mater.* **2011**, *10*, 502.
(3) Chen, Y.; Prociuk, A.; Perrine, T.; Dunietz, B. D. *Phys. Rev. B: Condens. Matter Mater. Phys.* **2006**, *74*, 245320.
(4) Kondo, H.; Kino, H.; Nara, J.; Ohno, T. *Appl. Surf. Sci.* **2008**, *254*, 7985.
(5) Salazar-Salinas, K.; Jauregui, L. A.; Kubli-Garfias, C.; Seminario, J. M. *J. Chem. Phys.* **2009**, *130*, 105101.
(6) Wagner, S.; Kisslinger, F.; Ballmann, S.; Schramm, F.; Chandrasekar, R.; Bodenstein, T.; Fuhr, O.; Secker, D.; Fink, K.; Ruben, M.; Weber, H. B. *Nat. Nanotechnol.* **2013**, *8*, 575.
(7) Liu, Z.-F.; Wei, S.; Yoon, H.; Adak, O.; Ponce, I.; Jiang, Y.; Jang, W.-D.; Campos, L. M.; Venkataraman, L.; Neaton, J. B. *Nano Lett.* **2014**, *14*, 5365.
(8) Wernsdorfer, W.; Sessoli, R. *Science* **1999**, *284*, 133.
(9) Leuenberger, M. N.; Loss, D. *Nature* **2001**, *410*, 789.
(10) Troiani, F.; Ghirri, A.; Affronte, M.; Carretta, S.; Santini, P.; Amoretti, G.; Piligkos, S.; Timco, G.; Winpenny, R. E. P. *Phys. Rev. Lett.* **2005**, *94*, 207208.
(11) Timco, G. A.; Carretta, S.; Troiani, F.; Tuna, F.; Pritchard, R. J.; Muryn, C. A.; McInnes, E. J. L.; Ghirri, A.; Candini, A.; Santini, P.; Amoretti, G.; Affronte, M.; Winpenny, R. E. P. *Nat. Nanotechnol.* **2009**, *4*, 173.
(12) Krull, C.; Robles, R.; Mugarza, A.; Gambardella, P. *Nat. Mater.* **2013**, *12*, 337.
(13) Mannini, M.; Pineider, F.; Sainctavit, P.; Danieli, C.; Otero, E.; Sciancalepore, C.; Talarico, A. M.; Arrio, M.-A.; Cornia, A.; Gatteschi, D.; Sessoli, R. *Nat. Mater.* **2009**, *8*, 194.
(14) Loth, S.; Baumann, S.; Lutz, C. P.; Eigler, D. M.; Heinrich, A. J. *Science* **2012**, *335*, 196.
(15) Khajetoorians, A. A.; Wiebe, J.; Chilian, B.; Lounis, S.; Blügel, S.; Wiesendanger, R. *Nat. Phys.* **2012**, *8*, 497.
(16) Spinelli, A.; Bryant, B.; Delgado, F.; Fernández-Rossier, J.; Otte, A. F. *Nat. Mater.* **2014**, *13*, 782.
(17) Bao, Z.; Lovinger, A. J.; Dodabalapur, A. *Appl. Phys. Lett.* **1996**, *69*, 3066.
(18) de Boer, R. W. I.; Stassen, A. F.; Craciun, M. F.; Mulder, C. L.; Molinari, A.; Rogge, S.; Morpurgo, A. F. *Appl. Phys. Lett.* **2005**, *86*, 262109.
(19) Hung, L. S.; Tang, C. W. *Appl. Phys. Lett.* **1999**, *74*, 3209.
(20) Parthasarathy, G.; Burrows, P. E.; Khalfin, V.; Kozlov, V. G.; Forrest, S. R. *Appl. Phys. Lett.* **1998**, *72*, 2138.
(21) Singh, V. P.; Singh, R. S.; Parthasarathy, B.; Aguilera, A.; Anthony, J.; Payne, M. *Appl. Phys. Lett.* **2005**, *86*, 082106.
(22) Gargiani, P.; Calabrese, A.; Mariani, C.; Betti, M. G. *J. Phys. Chem. C* **2010**, *114*, 12258.
(23) Yan, L.; Watkins, N. J.; Zorba, S.; Gao, Y.; Tang, C. W. *Appl. Phys. Lett.* **2001**, *79*, 4148.
(24) Craciun, M. F.; Rogge, S.; den Boer, M.-J. L.; Margadonna, S.; Prassides, K.; Iwasa, Y.; Morpurgo, A. F. *Adv. Mater.* **2006**, *18*, 320.
(25) Craciun, M. F.; Rogge, S.; Morpurgo, A. F. *J. Am. Chem. Soc.* **2005**, *127*, 12210.
(26) Giovannetti, G.; Brocks, G.; van den Brink, J. *Phys. Rev. B: Condens. Matter Mater. Phys.* **2008**, *77*, 035133.
(27) Filibian, M.; Carretta, P.; Mozzati, M. C.; Ghigna, P.; Zoppellaro, G.; Ruben, M. *Phys. Rev. Lett.* **2008**, *100*, 117601.
(28) Misiorny, M.; Hell, M.; Wegewijs, M. R. *Nat. Phys.* **2013**, *9*, 801.
(29) Khajetoorians, A. A.; Wiebe, J.; Chilian, B.; Wiesendanger, R. *Science* **2011**, *332*, 1062.
(30) Fransson, J. *Non-Equilibrium Nano-Physics*; Springer: New York, 2010.
(31) König, J.; Martinek, J. *Phys. Rev. Lett.* **2003**, *90*, 166602.
(32) Fransson, J.; Ren, J.; Zhu, J.-X. *Phys. Rev. Lett.* **2014**, *113*, 257201.
(33) Imamura, H.; Bruno, P.; Utsumi, Y. *Phys. Rev. B: Condens. Matter Mater. Phys.* **2004**, *69*, 121303.
(34) Heinrich, B. W.; Ahmadi, G.; Müller, V. L.; Braun, L.; Pascual, J. I.; Franke, K. J. *Nano Lett.* **2013**, *13*, 4840.
(35) Heinrich, B. W.; Braun, L.; Pascual, J. I.; Franke, K. J. *Nano Lett.* **2015**, *15*, 4024.
(36) Coronado, E.; Day, P. *Chem. Rev.* **2004**, *104*, 5419.
(37) Chen, X.; Fu, Y.-S.; Ji, S.-H.; Zhang, T.; Cheng, P.; Ma, X.-C.; Zou, X.-L.; Duan, W.-H.; Jia, J.-F.; Xue, Q.-K. *Phys. Rev. Lett.* **2008**, *101*, 197208.
(38) Perrin, M. L.; Frisenda, R.; Koole, M.; Seldenthuis, J. S.; Gil, J. A. C.; Valkenier, H.; Hummelen, J. C.; Renaud, N.; Grozema, F. C.; Thijssen, J. M.; Dulić, D.; van der Zant, H. S. J. *Nat. Nanotechnol.* **2014**, *9*, 830.

DOI: 10.1021/acs.nanolett.6b00628
Nano Lett. 2016, 16, 2824−2829